Available online at www.sciencedirect.com
ScienceDirect
Trans. Nonferrous Met. Soc. China 34(2024) 1789−1803
Transactions of Nonferrous Metals Society of China
www.tnmsc.cn

Effect of lithium carbonate solution sealing treatment on corrosion resistance of anodized AA2099-T83 alloy

Peng-zhou ZHU[1,2], Yan-long MA[1], Wei-jiu HUANG[1,2],
Meng-ting ZOU[1], Bing-yuan YANG[1], Yi LIAO[3], Zhao-yuan LIANG[4]

1. College of Materials Science and Engineering, Chongqing University of Technology, Chongqing 400054, China;
2. College of Materials Science and Engineering, Chongqing University, Chongqing 400044, China;
3. College of Economics and Business Administration, Chongqing University of Education, Chongqing 400067, China;
4. Zhongke (Guangdong) Refinery & Petrochemical Company Limited, Zhanjiang 524076, China

Received 29 November 2022; accepted 10 August 2023

Abstract: In order to develop a new surface treatment technology for aluminum−lithium alloys, an AA2099-T83 alloy was anodized in a tartaric−sulfuric acid bath and then post-treated in lithium carbonate (Li_2CO_3) solutions of different temperature−concentration combinations. The results show that the post-treatment in Li_2CO_3 solutions can greatly improve corrosion resistance of the anodized alloy (withstanding up to 1300 h of neutral salt spray test). It is found that the sealing process is distinctly different for high-temperature/low-concentration and low-temperature/high-concentration combinations. Specifically, the anodic film is only partially sealed in high-temperature mode but more fully sealed in low-temperature mode. The mechanism for the high corrosion resistance of the treated alloy is ascribed to the barrier effect of the sealing products (i.e., Li−Al−LDH and/or boehmite) on the surface and in the interiors of the anodic film.

Key words: aluminum−lithium alloy; anodizing; corrosion resistance; lithium carbonate; Li−Al−LDH; sealing treatment

1 Introduction

Advanced aluminum−lithium (Al−Li) alloys have various advantages over conventional aluminum alloys, including a considerably greater specific strength [1,2]. Significantly, these alloys have emerged as viable substitutes for conventional 2xxx and 7xxx aluminum alloys within the aerospace sector. Currently, Al−Li alloys such as AA2196, AA2198, AA2060, and AA2099 have been effectively employed in prominent commercial aircraft, including the Airbus A380, Boeing B777-X, and COMAC C919, for the fabrication of crucial components such as fuselage skin, stringers, and floor beams [3−5]. Moreover, Al−Li alloys exhibit promising potential for deployment in the construction of rocket fuel tanks [6]. Pertinent studies have extensively characterized the impact of alloying constituents and impurities on the microstructural diversity of Al−Li alloys [7−9]. Consequently, similar to other high-strength aerospace aluminum alloys, Al−Li alloys are susceptible to localized corrosion in environments containing chloride ions [10,11]. Anodizing treatments are commonly employed in the aerospace industry to enhance the corrosion resistance of aluminum alloys [12]. Chromic acid anodizing (CAA), the most widely used method in the past, offers the highest corrosion resistance

Corresponding author: Yan-long MA, Tel: +86-13594093263, E-mail: myl@cqut.edu.cn;
Wei-jiu HUANG, Tel: +86-13594310898, E-mail: Huangweijiu@cqut.edu.cn
DOI: 10.1016/S1003-6326(24)66507-6

among anodizing treatments [13]. However, due to the toxic nature of hexavalent chromium, CAA is no longer permitted in many countries [14,15]. Therefore, numerous initiatives have been undertaken to develop high-performance and ecologically friendly anodizing procedures, such as the tartaric−sulfuric acid anodizing (TSA) process developed in Europe at the beginning of this century [16−18]. Nevertheless, the unique composition and microstructure of Al−Li alloys present new challenges for surface treatment techniques. Previous research on the anodizing behavior of Al−Li alloys in TSA baths has revealed the dissolution of most constituent particles, resulting in significant cavity defects within the anodic layer [19,20]. Consequently, these cavity defects adversely affect the corrosion resistance. Therefore, proper sealing of the anodic coating is imperative to further enhance the corrosion resistance of anodized Al−Li alloys.

The corrosion resistance of aluminum alloys can be improved by the formation of layered double hydroxides (LDHs) on bare or anodized surfaces, as supported by a large amount of literature [21,22]. LDHs, because of their unique structure, not only serve as a barrier against corrosive media but also exhibit an anion-exchange capability. The intercalation of Al^{3+} with other divalent cations M^{2+} (where M=Mg, Co, Ni, and Zn) gives rise to various LDH systems. However, the high Gibbs free energy and stringent preparation requirements, such as elevated temperature and extended processing time, pose significant limitations to the formation of conventional LDH systems [23,24]. However, interestingly, the presence of lithium ions in the interstitial sites of the $Al(OH)_3$ lattice may lead to the development of a distinctive LDH system known as Li−Al−LDH [25]. Li−Al−LDH exhibits a lower formation Gibbs free energy than other systems, such as Zn−Al−LDH, enabling its more rapid and accessible preparation at lower temperatures [26,27]. MATA et al [28] treated an anodized AA2024 alloy with a lithium nitrate-based solution at temperatures ranging from 25 to 95 °C, resulting in the formation of Li−Al−LDH on the anodic film. Subsequently, they observed excellent corrosion resistance by immersing the Li−Al−LDH film for 30 min in a solution containing VO^{3-} to upload corrosion inhibitors. Moreover, YANG et al [29] employed a similar approach as MATA et al [28], with the exception of the corrosion inhibitor uploading process, on an anodized Al−Li alloy. Remarkably, the treated alloy exhibited exceptional corrosion resistance, passing the 1000 h neutral salt spray test. The improved corrosion resistance was attributed to the sealing effect of boehmite and/or LDHs formed within the nanopores and on the surface of the anodic film. Furthermore, the film/alloy system demonstrated remarkable self-healing capabilities.

The relevant literature [30,31] indicates that the anodic film formed on Al−Li alloys can be effectively sealed by the formation of Li−Al−LDH in lithium salt solutions. Interestingly, the corrosion resistance of the treated Al−Li alloy can be significantly enhanced even without the addition of corrosion inhibitors. One effective strategy is to introduce anions that have a relatively high affinity for the aluminum hydroxide layers in LDH. This approach enables the sealing of the anodic film to occur more rapidly at lower temperatures, thus improving the overall corrosion resistance of the alloy. Previous studies [30−33] have demonstrated that CO_3^{2-} exhibits a higher affinity for aluminum hydroxide layers compared to NO_3^-. Consequently, it is possible to achieve a faster and lower-temperature sealing of anodized Al−Li alloys using a lithium carbonate (Li_2CO_3) solution compared to a lithium nitrate ($LiNO_3$) solution. In fact, research conducted by BUCHHEIT et al [34] suggests that Li−Al−LDH formation on aluminum alloy surfaces can occur at ambient temperature.

In this study, an investigation was conducted on the sealing process of anodized AA2099-T83 alloys in Li_2CO_3 solutions, considering the influence of temperature, lithium salt concentration, sealed anodic film structure, and corrosion resistance. The sealing process was found to consist of two stages: reaction-controlled sealing and diffusion-controlled sealing. Moreover, it is identified that corrosion resistance can be achieved under two distinct conditions: high-temperature/low-concentration and low-temperature/high-concentration combinations. Remarkably, the low-temperature mode, which is close to room temperature, exhibited the potential for achieving a more comprehensive sealing of the anodic film. Based on our findings, we proposed a novel surface treatment technology for Al−Li alloys using a post-treatment in lithium carbonate solutions. By

utilizing this approach, the corrosion resistance and sealing efficiency of Al−Li alloys can be significantly enhanced, paving the way for sustainable and cost-effective solutions in the industry.

2 Experimental

2.1 Materials and method

In this study, the substrate used was obtained from an extrusion profile of AA2099-T83 Al−Li alloy. The alloy composition (wt.%) consists of Li (1.8), Cu (2.7), Mg (0.3), Mn (0.3), Zn (0.7), Zr (0.09), and balanced Al. The pretreatment and TSA anodizing treatment followed the procedures outlined in previous studies [20]. To investigate the sealing treatment of the anodized alloy, experiments were conducted using Li_2CO_3 solution at varying concentrations (0.01, 0.03, 0.05, 0.07 and 0.1 mol/L) and sealing temperatures (25, 30, 50, 70, and 90 °C). Following pH adjustment of the solution to 12.0 using a 0.3 mol/L LiOH solution, all specimens underwent a post-treatment for 30 min. For comparison purpose, a sample that underwent standard anodizing (1500 s) and hot water sealing (HWS) was also included in the study.

2.2 Microstructure characterization

The microstructure of the specimens was characterized using a Zeiss Sigma HD™ scanning electron microscope equipped with an energy dispersive X-ray analyzer (EDS, Oxford). Additionally, the phase composition of the anodic film, both before and after the post-treatment, was analyzed using a PANalytical Empyrean Series 2 X-ray diffractometer with Cu K_α radiation. To prepare the cross-sections of the samples, ultra-microtomy (Leica Ultracut) was performed using a diamond knife. The Yvon RF5000 GD glow discharge spectrometer was employed to analyze the distribution of H, Al, O, S, Cu, and Li across the anodic film thickness before and after post-sealing.

2.3 Electrochemical measurement and corrosion resistance test

To assess the electrochemical properties of the anodized alloy specimens treated with different sealing methods, potentiodynamic polarization (PDP) and electrochemical impedance spectroscopy (EIS) measurements were conducted at room temperature ((25±1) °C) in a 0.05 mol/L NaCl solution, using a Gamry Interface 3000 system. For the PDP measurements, a scanning rate of 1 mV/s was employed to obtain data on the corrosion behavior of the specimens. The EIS measurements were performed over a frequency range from 10^5 to 10^{-2} Hz, with a sinusoidal perturbation of 10 mV applied relative to the open circuit potential (OCP). A saturated calomel electrode served as the reference electrode, a platinum plate as the counter electrode, and the sample with an exposed area of 2.25 cm^2 as the working electrode. The acquired EIS data were analyzed using Zsimp Win software for impedance fitting. To further examine localized corrosion behavior, the scanning vibrating electrode technique (SVET) was employed. This technique was carried out using a Princeton Versa SCAN Micro Area Electrochemical Test System in a 0.05 mol/L NaCl solution. The distance between the micro-electrode and the sample surface was adjusted to approximately 200 μm. The vibration frequency and amplitude were set to be 80 Hz and 30 μm, respectively. A 100 mm^2 (10 mm × 10 mm) area was scanned with a step size of 100 μm.

3 Results

3.1 Process optimization and structure characterization

Initially, the anodized alloy specimens underwent post-treatment using 25 different combinations of sealing temperature and Li_2CO_3 concentration. The corrosion current density (J_{corr}) and corrosion potential (φ_{corr}) of each specimen, obtained from PDP curves (refer to Supplementary Materials), are summarized in Table 1. The results reveal that at all sealing temperatures, the specimens treated with a 0.01 mol/L Li_2CO_3 solution exhibited relatively low J_{corr} values, with the lowst J_{corr} value at 90 °C. When the Li_2CO_3 concentration was increased to 0.03 mol/L, except for the specimen treated at 25 °C, all others demonstrated improved corrosion resistance with relatively low J_{corr} values. However, as the Li_2CO_3 concentration further increased to 0.05, 0.07, and 0.1 mol/L, the J_{corr} values tended to rise with increasing temperature. Particularly, at 0.1 mol/L Li_2CO_3, the J_{corr} showed a significant increase when the temperature exceeded 50 °C. Based on the findings presented in Table 1, it can be inferred that

Table 1 Corrosion potential (φ_{corr}) and corrosion current density (J_{corr}) derived from potentiodynamic polarization curves

Sample No.	Process parameter		J_{corr}/(A·cm^{-2})	φ_{corr}(vs SCE)/V
	Li_2CO_3 concentration/(mol·L^{-1})	Temperature/°C		
1	0.01	25	2.54×10^{-8}	−0.54
2		30	5.08×10^{-8}	−0.46
3		50	9.88×10^{-9}	−0.51
4		70	5.44×10^{-8}	−0.43
5		90	3.10×10^{-9}	−0.43
6	0.03	25	3.24×10^{-7}	−0.49
7		30	6.80×10^{-8}	−0.47
8		50	5.62×10^{-8}	−0.48
9		70	9.55×10^{-8}	−0.46
10		90	8.7×10^{-10}	−0.73
11	0.05	25	5.08×10^{-8}	−0.46
12		30	4.72×10^{-8}	−0.46
13		50	3.11×10^{-8}	−0.47
14		70	3.95×10^{-8}	−0.45
15		90	1.20×10^{-7}	−0.53
16	0.07	25	7.61×10^{-9}	−0.49
17		30	1.54×10^{-9}	−0.45
18		50	1.49×10^{-7}	−0.56
19		70	4.06×10^{-8}	−0.47
20		90	4.60×10^{-7}	−0.52
21	0.1	25	1.88×10^{-9}	−0.55
22		30	1.22×10^{-8}	−0.57
23		50	9.51×10^{-7}	−0.66
24		70	8.11×10^{-5}	−1.20
25		90	4.40×10^{-4}	−1.40

the anodized alloy can achieve high corrosion resistance through sealing in either a dilute solution at a relatively high temperature or a concentrated solution at a relatively low temperature. Notably, it was discovered that when the Li_2CO_3 concentration ranged from 0.05 to 0.1 mol/L, the anodic film could be effectively sealed at room temperature while maintaining high corrosion resistance. Considering cost considerations, 0.05 mol/L Li_2CO_3 was selected for further investigation. As a result, two groups of specimens were studied in detail: the high-temperature/low-concentration group (0.01 mol/L at 50, 70 and 90 °C) and the low-temperature/high-concentration group (0.05 mol/L at 25, 30 and 50 °C). These groups were chosen for further analysis based on their distinct sealing conditions.

Figure 1 shows the surface and cross-section morphologies of the anodic film after post-treatment, specifically under high-temperature/low-concentration combination conditions (0.01 mol/L Li_2CO_3) at various temperatures (50, 70 and 90 °C). The results demonstrate a typical lamellar surface morphology for all specimens, indicating the formation of a unique substance on the anodic film. It is important to note that the sealed anodic film exhibits a two-layer structure, maintaining the same thickness as the as-prepared anodic film (3.9 μm)

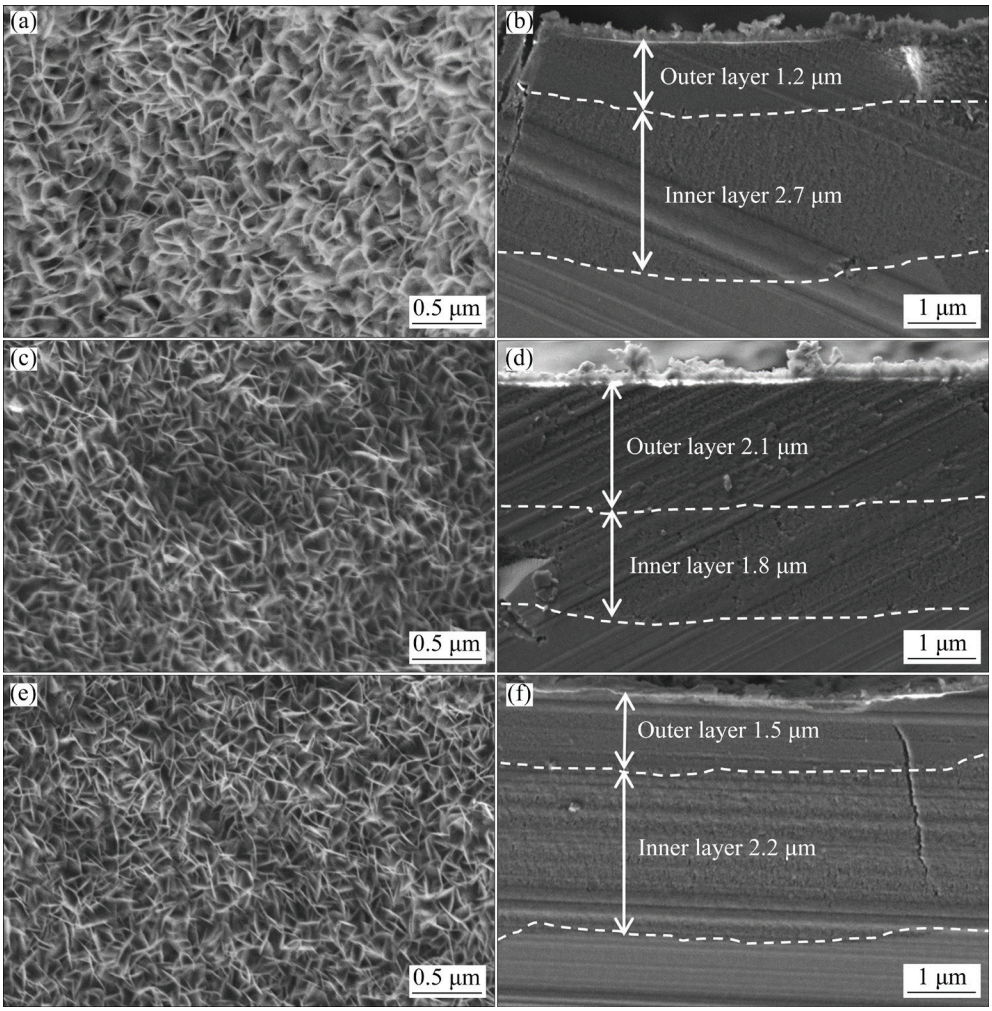

Fig. 1 Surface (a, c, e) and cross-section (b, d, f) morphologies of anodic film after post-treatment in 0.01 mol/L Li_2CO_3 solutions at different temperatures: (a, b) 50 °C; (c, d) 70 °C; (e, f) 90 °C

(referring to Supplementary Materials for further details). Notably, the lamellar structure observed on the anodic film surface corresponds to the uppermost layer, which has a thickness of a few hundred nanometers. The modified anodic film, which has a dense outer layer and a porous inner layer, lies beneath the lamellar structure. This two-layer structure of the anodic film suggests that the behavior of the sealing process differs in the outer and inner regions.

Figure 2 shows the surface and cross-section morphologies of the anodic film following post-treatment under low-temperature/high-concentration combination conditions (0.05 mol/L) at various temperatures (25, 30 and 50 °C). The surface morphology of the anodic film appears similar to what was observed in Fig. 1. However, significant differences emerge in the cross-section morphology of the sealed anodic film. Following the sealing process, the thickness of the anodic film increased by approximately 1.0 μm, while its morphology remained uniform throughout its thickness. It is important to note that the outermost layer, corresponding to the lamellar surface structure observed in Fig. 1, should still exist but may be obscured by the surface charge effect in Fig. 2. The variation in the structure of the sealed anodic film, as depicted in Figs. 1 and 2, suggests a disparity in the sealing process between the two sets of conditions.

Figure 3 shows the phase structure analysis results of the sealed anodic film under different conditions. For all samples, a peak is observed at 2θ of 29.0°, which corresponds to boehmite ($Al_2O_3·H_2O$) [35,36]. Furthermore, the low-temperature sealing group (0.05 mol/L Li_2CO_3 at 25,

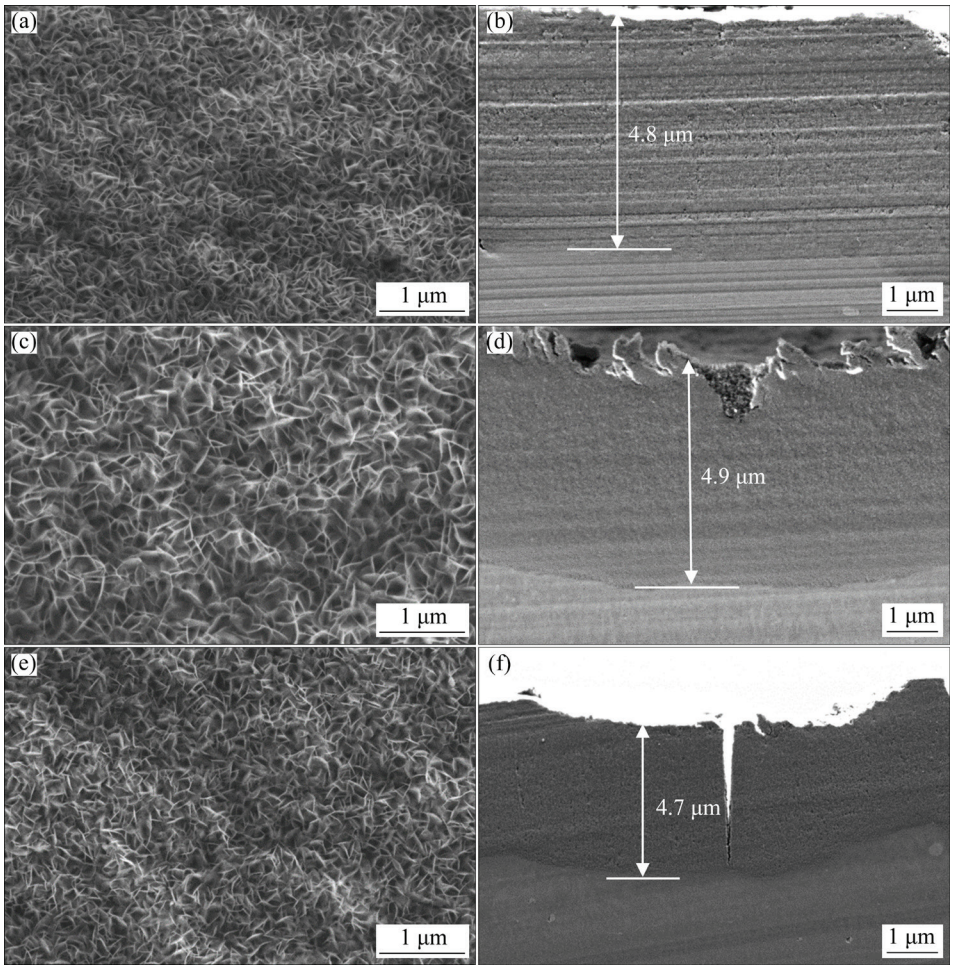

Fig. 2 Surface (a, c, e) and cross-section (b, d, f) morphologies of anodic film after post-treatment in 0.05 mol/L Li_2CO_3 solutions at different temperatures: (a, b) 25 °C; (c, d) 30 °C; (e, f) 50 °C

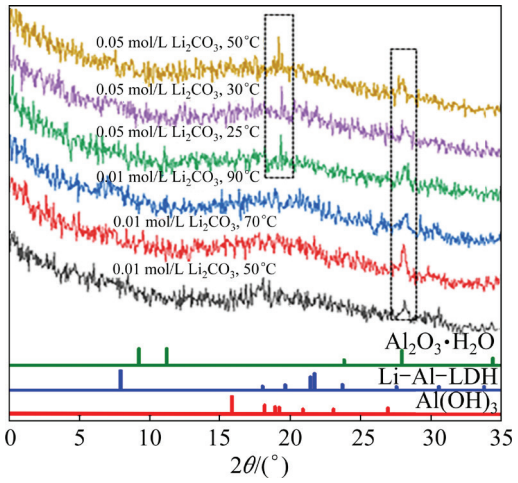

Fig. 3 XRD patterns of anodized alloys in different post-treatment conditions

30 and 50 °C) exhibits an additional peak at 2θ of approximately 20°, corresponding to Li−Al−LDH [37]. However, in the high-temperature group (0.01 mol/L Li_2CO_3 at 50, 70 and 90 °C), no observable peak associated with Li−Al−LDH is detected. Considering the similar surface morphology observed in Figs. 1 and 2, it can be assumed that the sealing products on all samples possess similarities. Thus, it is speculated that the sealing products formed in the high-temperature group may contain some amorphous Li−Al hydroxides in addition to boehmite.

In order to obtain a more comprehensive understanding of the sealing process under various conditions, compositional distribution analysis (Al, C, O, S, Cu, H, and Li) across the thickness of the anodic film was conducted for the TSA samples (the 0.01 mol/L Li_2CO_3, 50 °C sample; the 0.05 mol/L Li_2CO_3, 30 °C sample) using glow discharge optical emission spectroscopy (GDOES), as shown in Fig. 4. The sealing treatment significantly increased the concentrations of Li, O,

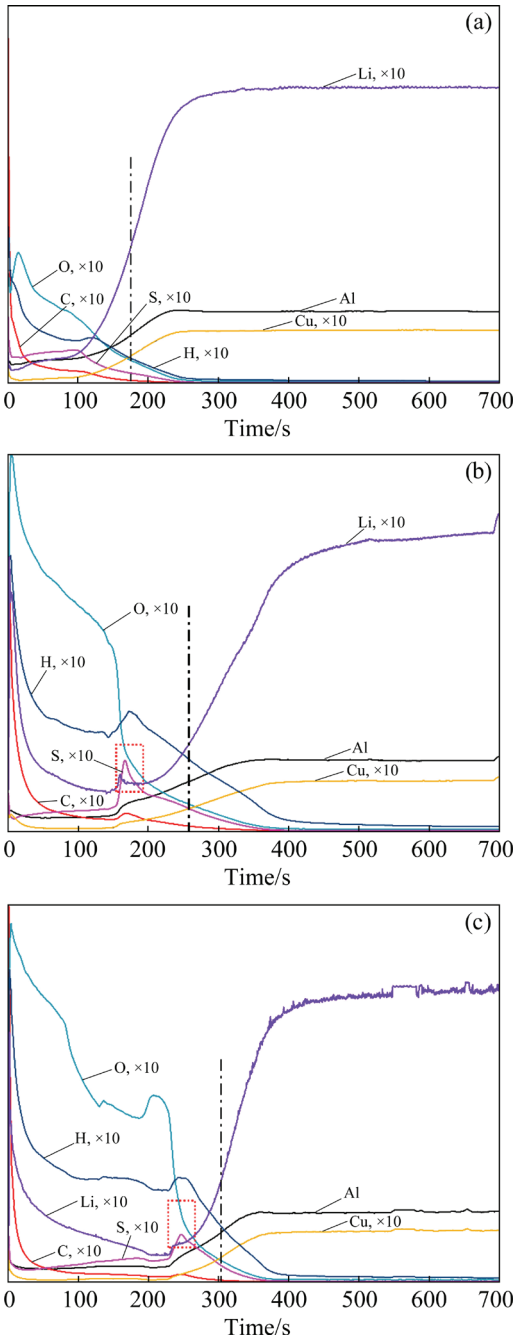

Fig. 4 GDOES depth profiles across different films: (a) TSA; (b) After post-treatment in 0.01 mol/L Li_2CO_3 solution at 50 °C; (c) After post-treatment in 0.05 mol/L Li_2CO_3 solution at 30 °C

H, and C in the anodic film, indicating the formation of Li−Al−LDH−CO_3 or amorphous Li−Al hydroxides on the surface and within the anodic film. It can be assumed that S primarily originates from the as-formed aluminum oxide, while Li is predominantly derived from the sealing products. In the outer regions of the anodic film, there is a depletion of S and an enrichment of Li, suggesting the transformation of aluminum oxide into sealing products. Near the interface between the film and the alloy, the simultaneous presence of S and Li peaks in Figs. 4(b) and (c) indicates the boundary between fully sealed regions of the anodic film and inadequately sealed regions. The proximity of this boundary to the film/alloy interface depends on the depth of the sealing. Therefore, the results indicate that the anodic film is more effectively sealed under conditions of low temperature and high concentration. In addition, the pronounced S and Li peaks in the boundary region of Fig. 4(b) indicate a structural distinction between the outer and inner regions of the anodic film. In contrast, the S and Li peaks in the boundary region of Fig. 4(c) appear relatively flat, suggesting a more uniform sealing across the thickness of the film. These findings align with the cross-sectional views of the anodic film presented in Figs. 1 and 2.

3.2 Corrosion resistance

Figure 5 provides a comparison of the Bode plots for samples sealed in 0.01 mol/L Li_2CO_3 (Fig. 5(a)) and 0.05 mol/L Li_2CO_3 (Fig. 5(b)) solutions

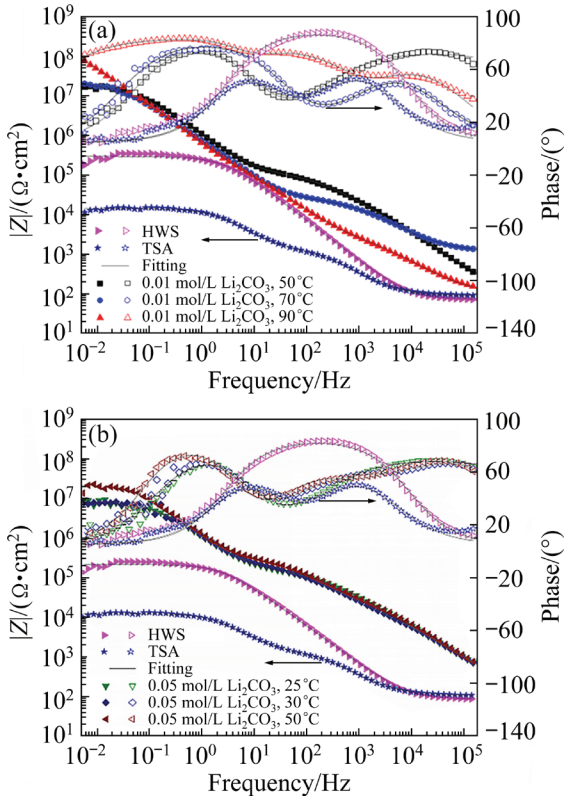

Fig. 5 Comparison of electrochemical impedance spectra taken from anodized alloy (TSA), after hot water sealing (HWS) and post-treatment in Li_2CO_3 solutions: (a) 0.01 mol/L Li_2CO_3, 50, 70 and 90 °C; (b) 0.05 mol/L Li_2CO_3, 25, 30 and 50 °C

at different temperatures, with TSA and HWS samples serving as references. Generally, the impedance moduli of the lithium salt sealing samples are significantly higher than those of the TSA and HWS samples, indicating superior corrosion resistance in the lithium salt sealing samples. To fit the Bode plots, an equivalent circuit as illustrated in Fig. 6 was utilized. This circuit comprises resistances for the electrolyte (R_s), the outer sealed anodic film (or the porous layer before sealing) denoted as R_p, and the inner sealed anodic film (or the barrier layer before sealing) represented by R_b. Furthermore, the circuit includes capacitances (Q_p and Q_b) corresponding to these resistances. In the case of localized corrosion, the charge transfer resistance (R_{ct}) and its corresponding capacitance (Q_{dl}) are also considered. By fitting the EIS spectra, the parameters for the equivalent circuits presented in Fig. 5 were obtained, as shown in Table 2.

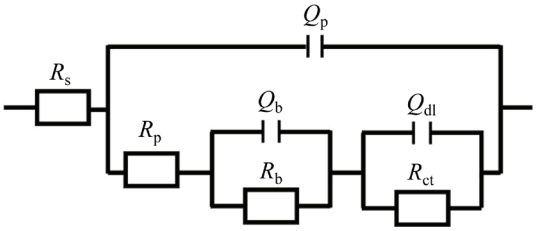

Fig. 6 Equivalent circuit used to fit electrochemical impedance spectra shown in Fig. 5

As per previous literature [38], the impedance modulus at 0.01 Hz ($|Z|_{0.01\ Hz}$) is a quantitative indicator of the overall stability and corrosion resistance of the film on the metal surface. In Fig. 7, the $|Z|_{0.01\ Hz}$ values of various samples after immersing in a NaCl solution for up to 1000 h were compared. The $|Z|_{0.01\ Hz}$ values of the TSA and HWS samples revealed a continuous decrease as immersion time increased, suggesting a compromised film structure during the immersion process. In contrast, the $|Z|_{0.01\ Hz}$ values of the samples sealed with lithium salt remained nearly unchanged throughout the immersion period. This consistent $|Z|_{0.01\ Hz}$ value indicates that the samples sealed with lithium salt possess superior corrosion resistance, even after the prolonged exposure to corrosive environments. These results further highlight the effectiveness of the lithium salt sealing treatment in enhancing the corrosion resistance of the anodic films on the metal surface.

In order to investigate the behavior of the 0.01 mol/L Li_2CO_3, 50 °C sample in a 0.05 mol/L NaCl solution, scanning vibrating electrode technique (SVET) analysis was conducted for a duration of 120 h. Figure 8 presents surface current density maps obtained at different immersion time, with dashed lines indicating surface scratches. Upon extended immersion time, localized corrosion sites labeled as *A*, *B*, and *C* were identified as current density spikes occurring in the scratched areas. Notably, the current density at these specific localized corrosion sites consistently decreased as the immersion time increased, eventually reaching background levels. This observation suggests that these localized corrosion sites underwent passivation after initiation. These findings align with previous research regarding the post-sealing effects on the same alloy in lithium nitrate-based solutions [29].

Table 2 Equivalent circuit parameters of samples under different conditions

Condition	R_s/ ($\Omega\cdot cm^2$)	R_p/ ($\Omega\cdot cm^2$)	Q_p/ ($\Omega^{-1}\cdot cm^{-2}\cdot s^n$)	n_p	R_b/ ($\Omega\cdot cm^2$)	Q_b/ ($\Omega^{-1}\cdot cm^{-2}\cdot s^n$)	n_b	R_{ct}/ ($\Omega\cdot cm^2$)	Q_{dl}/ ($\Omega^{-1}\cdot cm^{-2}\cdot s^n$)	n_{dl}
0.01 mol/L Li_2CO_3, 50 °C	65.00	2.87×10^5	3.93×10^{-6}	0.82	7.40×10^6	3.88×10^{-7}	0.93	−	−	−
0.01 mol/L Li_2CO_3, 70 °C	48.64	8.03×10^5	2.29×10^{-7}	0.41	9.28×10^6	1.10×10^{-6}	0.84	−	−	−
0.0 1 mol/L Li_2CO_3, 90 °C	57.35	9.19×10^4	6.52×10^{-7}	0.75	7.14×10^7	2.05×10^{-7}	1	−	−	−
0.05 mol/L Li_2CO_3, 25 °C	71.68	3.15×10^4	5.67×10^{-7}	0.84	1.04×10^7	6.64×10^{-7}	0.95	−	−	−
0.05 mol/L Li_2CO_3, 30 °C	43.87	4.34×10^5	3.85×10^{-8}	0.88	6.80×10^6	5.46×10^{-7}	0.99	−	−	−
0.05 mol/L Li_2CO_3, 50 °C	57.20	1.58×10^6	3.85×10^{-7}	0.70	7.09×10^6	9.12×10^{-7}	1	−	−	−
HWS−TSA	52.94	4.64×10^4	9.26×10^{-7}	0.91	2.42×10^5	3.22×10^{-6}	0.99	−	−	−
TSA	67.14	0.70×10^3	2.68×10^{-6}	1	2.01×10^4	5.68×10^{-8}	0.96	0.34×10^4	1.80×10^{-5}	0.85

n, n_p, n_b and n_{dl} represent exponents of the constant phase elements

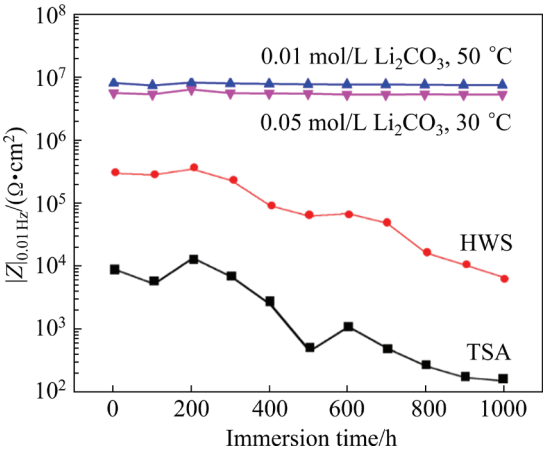

Fig. 7 Variation of $|Z|_{0.01\ Hz}$ of different coating systems with immersion time when exposed to NaCl solution

In order to assess the long-term corrosion resistance of the anodized alloy following lithium salt sealing, a neutral salt spray test (NSST) was conducted. To minimize the exposure time, the initial thickness of the as-prepared anodic film was reduced from 3.9 to 2.8 μm. Figure 9 provides a cross-section morphology of the samples (TSA; HWS; 0.01 mol/L Li_2CO_3, 50 °C; 0.05 mol/L, 30 °C), illustrating film thicknesses of 2.8, 2.8, 2.9, and 3.9 μm, respectively.

Figure 10 presents a comparison of the macroscopic morphologies of different samples exposed to NSST for varying durations. As expected, severe localized corrosion was initially observed on the TSA sample, followed by the HWS sample. However, after 1300 h of exposure, the 0.01 mol/L Li_2CO_3, 50 °C sample exhibited no signs of corrosion, indicating exceptional corrosion resistance. Upon reaching 500 h of exposure, a corrosion pit was observed on the 0.05 mol/L Li_2CO_3, 30 °C sample. However, as the exposure time was extended, the corrosion of this pit progressed at a remarkably slow rate, and no additional corrosion pits formed elsewhere. It is hypothesized that this corrosion depression may have resulted from the failure of the resin at the edge of the sample rather than the failure of the anodic film itself.

Figure 11 shows the surface and cross-section morphologies of these samples experiencing a 1300 h NSST. Surface analysis revealed the presence of porous or particulate features on the TSA and HWS samples, and the increase in film thickness from 2.8 (Fig. 9) to 8.1 and 10.5 μm (Fig. 11), respectively. The increase in film thickness was attributed to the deposition of corrosion

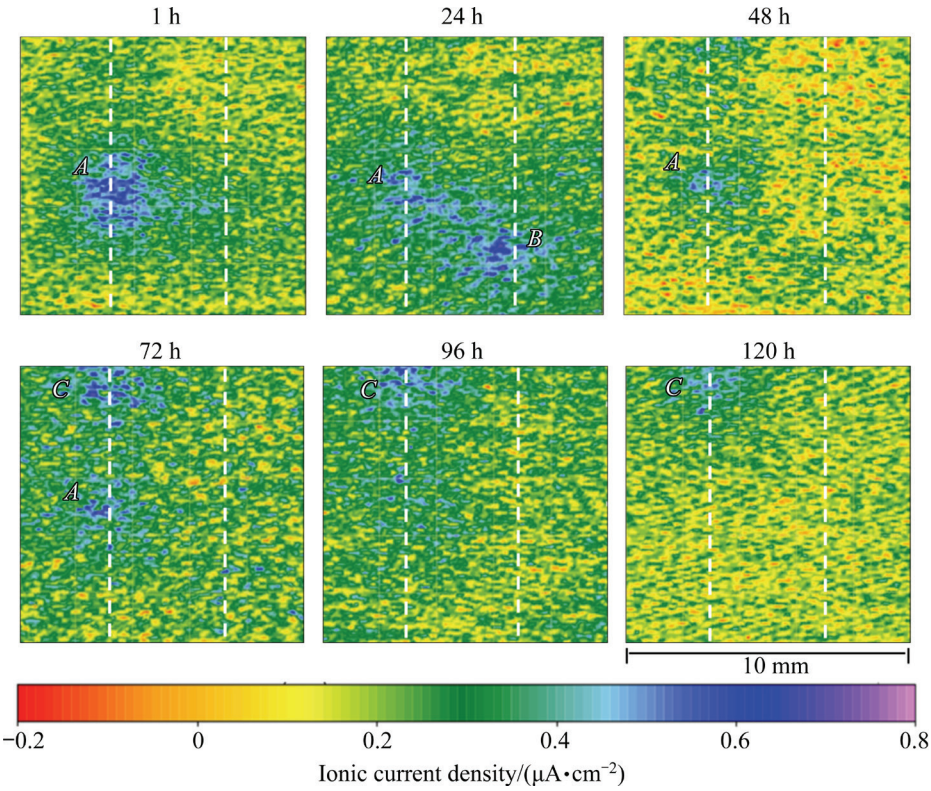

Fig. 8 SVET maps of 0.01 mol/L Li_2CO_3, 50 °C sample recorded during immersion in 0.05 mol/L NaCl solution for different periods of time (The dashed lines indicate the location of the artificial scratches)

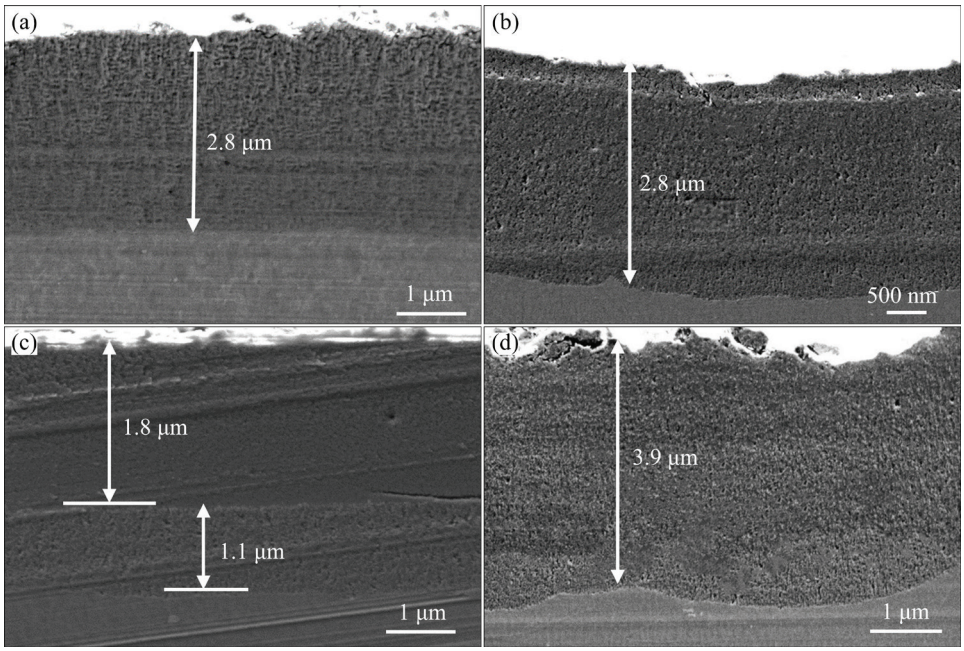

Fig. 9 Cross-section morphologies of different coating systems before neutral salt spray test: (a) TSA; (b) HWS; (c) 0.01 mol/L Li_2CO_3, 50 °C; (d) 0.05 mol/L Li_2CO_3, 30 °C

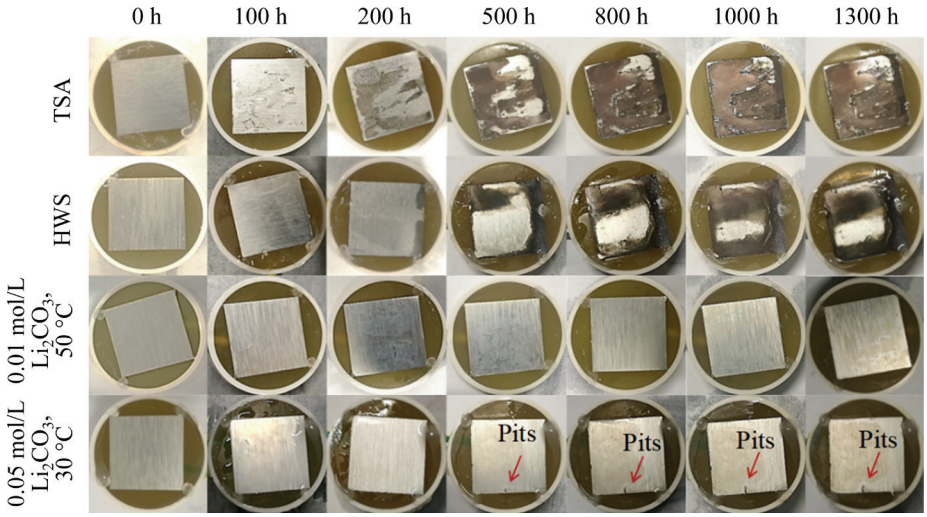

Fig. 10 Comparison of appearance of different samples exposed to neutral salt spray test for different time

products resulting from the corrosion attack on the alloy substrate beneath the anodic film. The localized corrosion sites deep within the alloy substrates (as labeled) confirm the stable propagation of the localized corrosion within the substrates. In contrast, the distinctive lamellar structure formed during lithium salt sealing process remained visually intact even after 1300 h of exposure. Furthermore, no significant increase in film thickness was observed. These observations indicate that the corrosion attack on the samples subjected to lithium salt sealing was weak.

4 Discussion

The effects of sealing temperature and lithium salt concentration on anodic film sealing were investigated in this study. Two optimal conditions of a high-temperature/low-concentration and a low-temperature/high-concentration were discovered. The sealing process was divided into two stages, with the initial stage involving the penetration of the sealing solution through nanopores in the anodic film and the reaction with alumina oxide to form

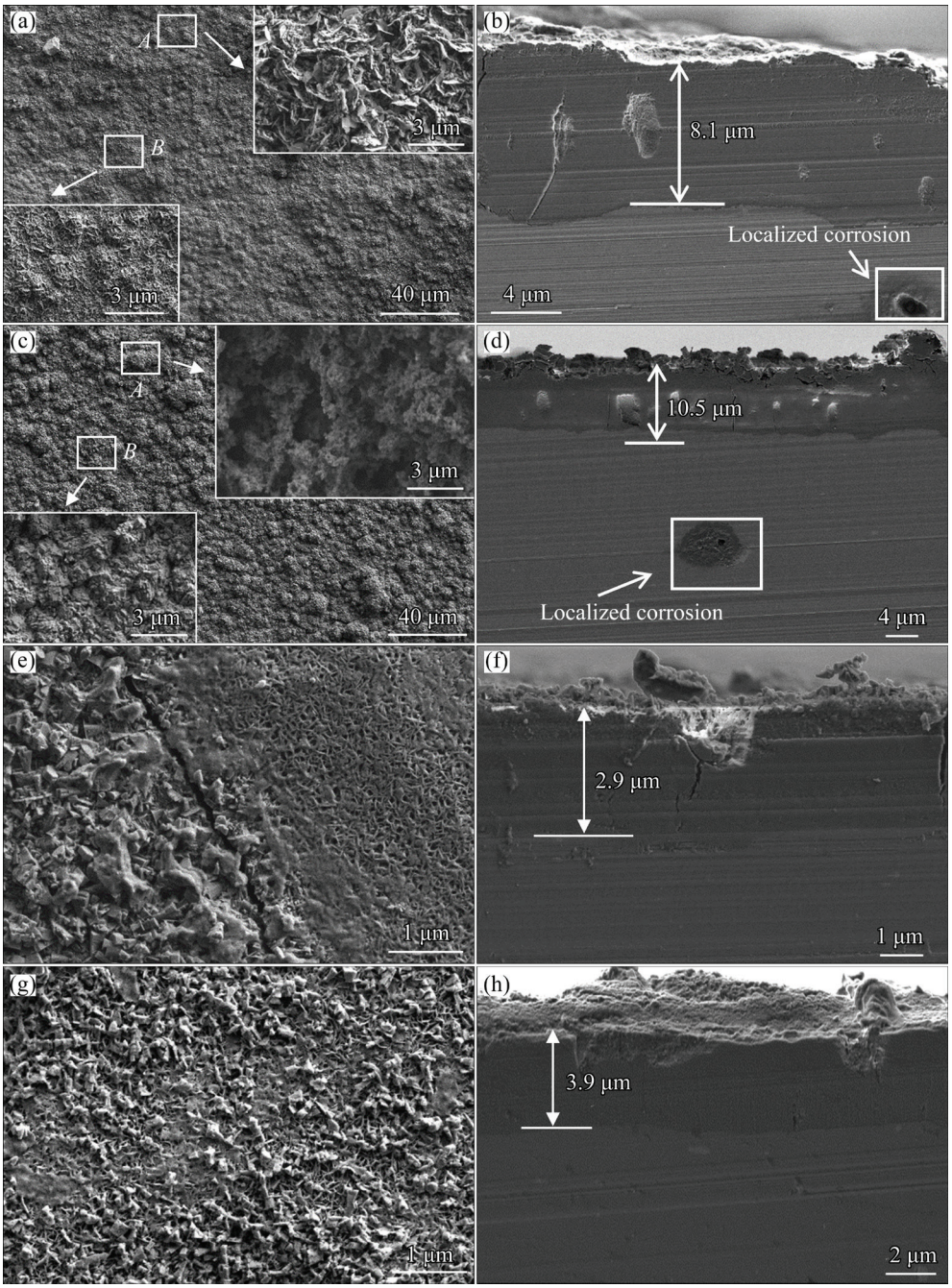

Fig. 11 Surface (a, c, e, g) and cross-section (b, d, f, h) morphologies of different samples exposed to NSST for 1300 h: (a, b) TSA; (c, d) HWS; (e, f) 0.01 mol/L Li_2CO_3, 50 °C; (g, h) 0.05 mol/L Li_2CO_3, 30 °C

sealing products. In the later stage, sealing products accumulated in nanopores, making ion exchange more challenging and controlling the sealing reaction by diffusion. As the diffusion distance increased towards the film interior, the sealing reactions became more difficult. However, the specific sealing process and resulting film structure varied significantly for different combinations of temperature and concentration. For the high-temperature/low-concentration pairing, sealing product nucleation rates were low, but their growth rates were high, leading to the coarsening of sealing product granules. These granules obstructed nanopores, limiting ion exchange and resulting in a two-layer film structure with minimal increase in thickness (Fig. 1). On the other hand, the low-temperature/high-concentration pairing exhibited high nucleation rates but low growth rates, resulting in sealing products with finer granules. This allowed the maintenance of inward diffusion of sealing

species and outward diffusion of Al^{3+} species, leading to a relatively uniform structure of the sealed anodic film across its thickness and an increase in film thickness (Fig. 2). These observations are supported by GDOES analysis (Fig. 4), which demonstrates that sealing products (indicated by the enrichment of Li, O, and H, but depletion of S) are distributed more uniformly and deeply throughout the film thickness in the low-temperature/high-concentration sample compared to the high-temperature/low concentration sample.

Different from the previous studies utilizing a lithium nitrate solution [29], the sealing process described in this research relies on a lithium carbonate solution. Furthermore, unlike previous research that focused solely on the influence of temperature on the sealing process, in this study, the combined effect of temperature and lithium salt concentration was considered, leading to the identification of two varieties of optimal conditions. Previous research indicated that satisfactory corrosion resistance could only be achieved at high temperatures, such as 70 and 90 °C [29]. In contrast, the current study demonstrates that excellent corrosion resistance can be attained at room temperatures, such as 25 and 30 °C, when relatively high concentrations of lithium salt, for example, 0.05 and 0.07 mol/L, are employed. Tables 1 and 2 present evidences that the corrosion resistance of alloy samples treated with the low-temperature/high-concentration combinations are comparable to or even superior to those treated with the high-temperature/low-concentration combinations.

Further investigation is warranted to understand the mechanism underlying the high corrosion resistance of the anodized alloy sealed with lithium carbonate, particularly in the case of the low-temperature/high-concentration combination. One contributing factor is the formation of Li−Al−LDH and/or boehmite, as well as the self-healing property of the film/alloy system [29]. Additionally, the more thorough sealing of the anodic film in the interior regions at low temperatures and the increase in film thickness after sealing likely contribute to the enhanced corrosion resistance. However, unlike NO_3^- ions in Li−Al−LDH−NO_3^-, which can be exchanged for Cl^-, CO_3^{2-} ions in Li−Al−LDH−CO_3^{2-} cannot be exchanged for Cl^- due to their higher affinity for hydroxide layers. Therefore, the corrosion protection mechanism associated with Cl^- ion capture in Li−Al−LDH is not applicable to the lithium carbonate system. The self-healing effect is only activated in the event of damage to the coating system. Based on these observations, it is concluded that the high corrosion resistance of the anodized alloy sealed with lithium carbonate primarily stems from the barrier effect of the sealing products, such as Li−Al−LDH and/or boehmite, on the surface and in the interior of the anodic film. Considering the reduced film thickness, it appears that the corrosion performance of the anodized alloy sealed with lithium carbonate surpasses that of the anodized alloy sealed with lithium nitrate (Fig. 9). In summary, lithium carbonate sealing offers a high-performance, environmentally-friendly, and promising surface treatment process for achieving superior corrosion resistance in anodized alloys.

5 Conclusions

(1) The anodized AA2099-T83 alloy can be successfully sealed using lithium carbonate solutions under different temperature−concentration combination conditions. Specifically, when the Li_2CO_3 solution concentration is 0.05 mol/L or higher and a sealing duration of 30 min at room temperature, the alloy specimen with an anodic film thickness of 2.8 μm exhibits remarkable durability, enduring 1300 h of NSST.

(2) The sealing process significantly depends on the temperature−concentration combination utilized. In the high-temperature/low-concentration combination, the outer regions of the anodic film experience more comprehensive sealing compared to the inner part, resulting in a two-layer sealing structure and no change in film thickness. On the other hand, in the low-temperature/high-concentration combination, the anodic film is uniformly sealed and the film thickness is increased.

(3) In the context of low-temperature/high-concentration combinations, the corrosion resistance of the alloy is found to be comparable or even superior to that achieved through high-temperature/low-concentration combinations. The exceptional corrosion resistance is primarily attributed to the barrier effect created by the sealing products, such as Li−Al−LDH and/or boehmite, on the surface and in the interior of the anodic film. These sealing products effectively prevent corrosive

agents from reaching the underlying alloy, thereby enhancing the overall corrosion resistance of the alloy.

CRediT authorship contribution statement

Peng-zhou ZHU: Investigation, Data curation, Writing − Original draft, Writing − Review & editing; **Yan-long MA:** Project administration, Validation, Data curation, Writing − Review & editing; **Wei-jiu HUANG:** Supervision, Project administration; **Meng-ting ZOU:** Investigation, Software, Visualization; **Bing-yuan YANG:** Investigation, Conceptualization; **Yi LIAO:** Methodology, Investigation; **Zhao-yuan LIANG:** Methodology, Visualization, Investigation.

Declaration of competing interest

The authors declare that they have no known competing financial interests or personal relationships that could have appeared to influence the work reported in this paper.

Acknowledgments

This work was supported by the Chongqing Talent Plan: Leading Talents in Innovation and Entrepreneurship, China (No. CQYC201903051), the University Innovation Research Group of Chongqing, China (No. CXQT20023), the Chongqing Natural Science Foundation, China (No. CSTB2022NSCQ-MSX0326), the National Natural Science Foundation of China (No. 51871038), and the Basic Research and Frontier Exploration Project of Chongqing Science and Technology Commission, China (No. cstc2021ycjh-bgzxm0173).

Supplementary Materials

Supplementary Materials in this paper can be found at: http://tnmsc.csu.edu.cn/download/06-p1789-2022-1359-Supplementary_Materials.pdf.

References

[1] RIOJA R J, LIU J. The evolution of Al−Li base products for aerospace and space applications [J]. Metallurgical and Materials Transactions A, 2012, 43: 3325−3337.

[2] NAYAN N, GURAO N P, MURTY S V S N, JHA A K, PANT B, SHARMA S C, GEORGE K M. Microstructure and micro-texture evolution during large strain deformation of an aluminium−copper−lithium alloy AA 2195 [J]. Materials & Design, 2015, 65: 862−868.

[3] DURSUN T, SOUTIS C. Recent developments in advanced aircraft aluminium alloys [J]. Materials & Design (1980—2015), 2014, 56: 862−871.

[4] GAO Chong, MA Yue, TANG Lin-zhi, WANG Peng, ZHANG Xin. Microstructural evolution and mechanical behavior of friction spot welded 2198-T8 Al−Li alloy during aging treatment [J]. Materials & Design, 2017, 115: 224−230.

[5] HAN Bing, CHEN Yan-bin, TAO Wang, LI Hao, LI Li-qun. Microstructural evolution and interfacial crack corrosion behavior of double-sided laser beam welded 2060/2099 Al−Li alloys T-joints [J]. Materials & Design, 2017, 135: 353−365.

[6] RODGERS B I, PRANGNELL P B. Quantification of the influence of increased pre-stretching on microstructure−strength relationships in the Al−Cu−Li alloy AA2195 [J]. Acta Materialia, 2016, 108: 55−67.

[7] LIU Bing, ZHOU Xiao-rong, ZHANG Xin-xin. Filiform corrosion behaviour on machined AA7150 aluminium alloy [J]. Transactions of Nonferrous Metals Society of China, 2020, 30: 2056−2066.

[8] JI Yuan-yuan, XU Yun-ze, ZHANG Bin-bin, BEHNAMIAN Y, XIA Da-hai, HU Wen-bin. Review of micro-scale and atomic-scale corrosion mechanisms of second phases in aluminum alloys [J]. Transactions of Nonferrous Metals Society of China, 2021, 31: 3205−3227.

[9] WEN Feng, CHEN Ji-qiang, HAN Shuang, ZHOU Zi-xiang, ZHONG Shi-biao, ZHANG Ying-hui, LI Wei-rong, GUAN Ren-guo. Effect of crystal orientations and precipitates on corrosion behavior of Al−Cu−Li single crystals [J]. Transactions of Nonferrous Metals Society of China, 2022, 32: 3887−3900.

[10] MA Y, ZHOU X, HUANG W, THOMPSON G E, ZHANG X, LUO C, SUN Z. Localized corrosion in AA2099-T83 aluminum–lithium alloy: The role of intermetallic particles [J]. Materials Chemistry and Physics, 2015, 161: 201−210.

[11] MA Y, ZHOU X, LIAO Y, YI Y, WU H, WANG Z, HUANG W. Localised corrosion in AA 2099-T83 aluminium−lithium alloy: The role of grain orientation [J]. Corrosion Science, 2016, 107: 41−48.

[12] BOISIER G, PEBERE N, DRUEZ C, VILLATTE M, SUEL S. FESEM and EIS study of sealed AA2024 T3 anodized in sulfuric acid electrolytes: Influence of tartaric acid [J]. Journal of the Electrochemical Society, 2008, 155: C521−C529.

[13] EICHINGER E, OSBORNE J, CLEAVE T V. Hexavalent chromium elimination: An aerospace industry progress report [J]. Metal Finishing, 1997, 95: 36−41.

[14] WU Liang, WU Jia-hao, ZHANG Ze-yu, ZHANG Cheng, ZHANG Yu-xin, TANG Ai-tao, LI Ling-jie, ZHANG Gen, ZHENG Zhi-cheng, ATRENS A, PAN Fu-sheng. Corrosion resistance of fatty acid and fluoroalkylsilane-modified hydrophobic Mg−Al LDH films on anodized magnesium alloy [J]. Applied Surface Science, 2019, 487: 569−580.

[15] WU Liang, DING Xing-xing, ZHENG Zhi-cheng, MA Yan-long, ATRENS A, CHEN Xiao-bo, XIE Zhi-hui, SUN De-en, PAN Fu-sheng. Fabrication and characterization of an actively protective Mg−Al LDHs/Al_2O_3 composite coating on magnesium alloy AZ31 [J]. Applied Surface Science, 2019, 487: 558−568.

[16] DOMINGUES L, FERNANDES J C S, BELO M D, FERREIRA M G S, GUERRA-ROSA L. Anodising of Al

2024-T3 in a modified sulphuric acid/boric acid bath for aeronautical applications [J]. Corrosion Science, 2003, 45: 149−160.

[17] WU H, MA Y, HUANG W, ZHOU X, LI K, LIAO Y, WANG Z, LIANG Z, LIU L. Effect of iron-containing intermetallic particles on film structure and corrosion resistance of anodized AA2099 alloy [J]. Journal of the Electrochemical Society, 2018, 165: 573−581.

[18] GLENN A M, HUGHES A E, MACRAE C M, WILSON N C, TORPY A, ZHOU X R. Observations on the early stages of corrosion on AA2099-T83 [J]. Microscopy and Microanalysis. 2020, 26: 821−836.

[19] LIANG Z, MA Y, LI K, LIAO Y, YANG B, LIU L, ZHU P. Formation of layered double hydroxides film on AA2099-T83 Al−Cu−Li alloy and its effect on corrosion resistance [J]. Surface and Coatings Technology, 2019, 378: 124967.

[20] ZHU P, MA Y, LI K, LIANG Z, YANG B, HUANG W, LIAO Y. Sealing of anodized AA 2099-T83 Al−Cu−Li alloy with layered double hydroxides for high corrosion resistance at reduced anodic film thickness [J]. Surface and Coatings Technology, 2020, 394: 125852.

[21] TEDIM J, KUZNETSOVA A, SALAK A N, MONTEMOR F, SNIHIROVA D, PILZ M, ZHELUDKEVICH M L, FERREIRA M G S. Zn−Al layered double hydroxides as chloride nanotraps in active protective coatings [J]. Corrosion Science, 2012, 55: 1−4.

[22] SHKIRSKIY V, KEIL P, HINTZE-BRUENING H, LEROUX F, STIMPFLING T, DRAGOE D, OGLE K, VOLOVITCH P. MoO_4^{2-} as a soluble inhibitor for Zn in neutral and alkaline solutions [J]. Corrosion Science, 2015, 99: 31−41.

[23] SHKIRSKIY V, KEIL P, HINTZE B H, LEROUX F, VIALAT P, LEFEVRE G, OGLE K, VOLOVIYCH P. Factors affecting MoO_4^{2-} inhibitor release from Zn_2Al based layered double hydroxide and their implication in protecting hot dip galvanized steel by means of organic coatings [J]. ACS Applied Materials & Interfaces, 2015, 7: 25180−25192.

[24] VISSER P, LUTZ A, MOL J M C, TERRYN H. Study of the formation of a protective layer in a defect from lithium-leaching organic coatings [J]. Progress in Organic Coatings, 2016, 99: 80−90.

[25] LIU Y W, VISSER P, ZHOU X R, LYON S B, HASHIMOTO T, CURIONI M, GHOLINIA A, THOMPSON G E, SMYTH G, GIBBON S R, GRAHAM D, MOL J M C, TERRYN H. Protective film formation on AA2024-T3 aluminum alloy by leaching of lithium carbonate from an organic coating [J]. Journal of the Electrochemical Society, 2016, 163(3): 45−53.

[26] LIU Jian-hua, SHI Hao-bo, YU Mei, DU Rong-tao, RONG Gang, LI Song-mei. Effect of divalent metal ions on durability and anticorrosion performance of layered double hydroxides on anodized 2A12 aluminum alloy [J]. Surface and Coatings Technology, 2019, 373: 56−64.

[27] CHEN Jia-ling, FANG Liang, WU Fang, ZENG Xian-guang, HU Jia, ZHANG Shu-fang, JIANG Bin, LUO Hai-jun. Comparison of corrosion resistance of MgAl−LDH and ZnAl−LDH films intercalated with organic anions ASP on AZ31 Mg alloys [J]. Transactions of Nonferrous Metals Society of China, 2020, 30: 2424−2434.

[28] MATA D, SERDECHNOVA M, MOHEDANO M, MENDIS C L, LAMAKA S V, TEDIM J, HACK T, NIXON S, ZHELUDKEVICH M L. Hierarchically organized Li−Al−LDH nano-flakes: A low-temperature approach to seal porous anodic oxide on aluminum alloys [J]. RSC Advances, 2017, 7: 35357−35367.

[29] YANG Bing-yuan, MA Yan-long, WU Hai-sheng, LIANG Zhao-yuan, LI Yu, WU Liang, SUN Li-dong. Improving corrosion resistance of anodized AA2099-T83 Al−Cu−Li alloy through post-treatment in a lithium nitrate-based solution [J]. Surface and Coatings Technology, 2022, 441: 128501.

[30] VISSER P, LIU Y W, ZHOU X R, HASHIMOTO T, THOMPSON G E, LYON S B, VAN-DER-VEN L G J, MOL A J M C, TERRYN H A. The corrosion protection of AA2024-T3 aluminium alloy by leaching of lithium-containing salts from organic coatings [J]. Faraday Discussions, 2015, 180: 511−526.

[31] SYU J H, UAN J Y, LIN M C, LIN Z Y. Optically transparent $Li−Al−CO_3$ layered double hydroxide thin films on an AZ31 Mg alloy formed by electrochemical deposition and their corrosion resistance in a dilute chloride environment [J]. Corrosion Science, 2013, 68: 238−248.

[32] LI Feng, SUN Xiang, SONG Liang, KANNAN M B, ZHANG Fen, CUI Lan-yue, ZOU Yu-hong, LI Shuo-qi, LIU Cheng-bao, ZENG Rong-chang. Influence of intermetallic Al−Mn particles on in-situ steam Mg−Al−LDH coating on AZ31 magnesium alloy [J]. Transactions of Nonferrous Metals Society of China, 2022, 32: 3926−3949.

[33] STIMPFLING T, VIALAT P, HINTZE-BRUENING H, KEIL P, SHKIRSKIY V, VOLOVITCH P, OGLE K, LEROUX F. Amino acid interleaved layered double hydroxides as promising hybrid materials for AA2024 corrosion inhibition [J]. European Journal of Inorganic Chemistry, 2016, 13(14): 2006−2016.

[34] BUCHHEIT R G, BODE M D, STONER G E. Corrosion-resistant, chromate-free talc coatings for aluminum [J]. Corrosion, 1994, 50(3): 205−214.

[35] ZHANG Cai-xia, LUO Xiao-hu, PAN Xin-yu, LIAO Li-ying, WU Xiao-song, LIU Ya-li. Self-healing Li−Al layered double hydroxide conversion coating modified with aspartic acid for 6N01 Al alloy [J]. Applied Surface Science, 2017, 394: 275−281.

[36] LI Yuan-yuan, LIU Jin-ping, HA Zhi-jie. Fabrication of boehmite AlOOH nanofibers by a simple hydrothermal process [J]. Materials Letters, 2006, 60: 3586−3590.

[37] WANG S L, LIN C H, YAN Y Y, WANG M K. Synthesis of Li/Al LDH using aluminum and LiOH [J]. Applied Clay Science, 2013, 72: 191−195.

[38] MA Y, ZHOU X, THOMPSON G E, ZHANG X, LUO C, CURIONI M, LIU H. Microstructural modification arising from alkaline etching and its effect on anodizing behavior of Al−Li−Cu alloy [J]. Journal of the Electrochemical Society, 2013, 160: 111−118.

碳酸锂溶液封闭处理对阳极氧化 AA2099-T83 合金耐蚀性能的影响

朱彭舟[1,2]，麻彦龙[1]，黄伟九[1,2]，邹梦婷[1]，杨炳元[1]，廖 益[3]，梁钊源[4]

1. 重庆理工大学 材料科学与工程学院，重庆 400054；
2. 重庆大学 材料科学与工程学院，重庆 400044；
3. 重庆第二师范学院 经济与工商管理学院，重庆 400067；
4. 中科(广东)炼油石化有限公司，湛江 524076

摘 要：为开发一种新型铝锂合金表面处理技术，将经酒石酸−硫酸阳极氧化后的 AA2099-T83 合金浸泡在不同温度−浓度组合的碳酸锂(Li_2CO_3)溶液中进行后处理。结果表明：经过 Li_2CO_3 溶液处理后，阳极氧化合金的耐蚀性能显著提高(耐中性盐雾试验长达 1300 h)。此外，高温/低浓度和低温/高浓度组合的封孔过程明显不同，在高温模式下阳极氧化膜仅部分封孔，而在低温模式下阳极氧化膜的封孔更加完全。封孔处理合金的高耐腐蚀性主要归因于在阳极氧化膜表面和内部形成的封孔产物(即 Li−Al−LDH 和/或勃姆石)对腐蚀介质的阻隔作用。

关键词：铝锂合金；阳极氧化；耐蚀性能；碳酸锂；锂−铝层状双氢氧化物；封闭处理

(Edited by Wei-ping CHEN)